New insights into the chemical activation of lignins and tannins using K_2CO_3—a combined thermoanalytical and structural study

Guizani, Chamseddine; Widsten, Petri; Siipola, Virpi; Paalijärvi, Riina; Berg, Jonathan; Pasanen, Antti; Kalliola, Anna; Torvinen, Katariina

Published in:
Carbon Letters

DOI:
10.1007/s42823-023-00601-4

E-pub ahead of print: 07/09/2023

Document Version
Publisher's final version

Carbon Letters
https://doi.org/10.1007/s42823-023-00601-4

Online ISSN 2233-4998
Print ISSN 1976-4251

ORIGINAL ARTICLE

New insights into the chemical activation of lignins and tannins using K_2CO_3—a combined thermoanalytical and structural study

Chamseddine Guizani[1] · Petri Widsten[1] · Virpi Siipola[1] · Riina Paalijärvi[1] · Jonathan Berg[1] · Antti Pasanen[1] · Anna Kalliola[1] · Katariina Torvinen[1]

Received: 10 July 2023 / Revised: 17 August 2023 / Accepted: 27 August 2023

Abstract
Engineering of activated carbons (ACs) through chemical activation of organic precursors has been extensively studied for a wide variety of biopolymers, biomasses, wastes and other fossil-based precursors. Despite huge efforts to engineer evermore performant and sustainable ACs, "searching-for-the-best-recipe" type of studies are more the rule than the exception in the published literature. Emerging AC applications related to energy and gas storage require strict control of the AC properties and a better understanding of the fundamentals underlying their engineering. In this study, we provide new insights into the K_2CO_3 chemical activation of plant-based polyphenols—lignins and tannins—through careful thermoanalytical and structural analyses. We showed for the the first time that the reactivity of polyphenols during K_2CO_3 chemical activation depends remarkably on their purity and structural properties, such as their content of inorganics, OH functionalities and average molecular weight. We also found that the burn-off level is proportional to the K_2CO_3/lignin impregnation ratio (IR), but only within a certain range—high impregnation ratios are not needed, unlike often reported in the literature. Furthermore, we showed for the first time that the K_2CO_3 chemical activation of different carbon surfaces from lignins and tannins can be modelled using simple global solid-state decomposition kinetics. The identified activation energies lay in the range of values reported for heterogenous gas-carbon surface gasification reactions (O_2-C, H_2O-C, or CO_2-C) in which the decomposition of C(O) surface complexes is the common rate-limiting step.

Keywords Lignins · Tannins · Structural analyses · Activated carbons · Chemical activation · K_2CO_3 · Reactivity · Kinetics

1 Introduction

Replacing fossil-based precursors by renewable ones is necessary to maintain a sustainable production of activated carbons (ACs) for different application areas, including energy storage, gas storage, and environmental remediation. Woody plants such as trees are rich sources of lignin and tannin polyphenols, which could be used as precursors for the next generation of renewable ACs.

In trees, lignin [1] is one of the major structural components of wood and occurs also in the bark. Lignins are polymers of phenylpropanoid units (Fig. 1) connected by ether (-C–O-) and carbon–carbon (C–C-) bonds. Softwoods such as pine and spruce consist mainly of guaiacyl (G) type of phenylpropanoid units and hardwoods such as eucalyptus and acacia of G and syringyl (S) units, respectively. Both types of wood may also contain *p*-hydroxyphenyl (H) type units.

The development of lignin recovery processes [2, 3] and novel biorefinery concepts [4] has increased the availability of technical lignins from chemical (kraft, soda and organosolv) pulping and hydrolysis lignin from biorefineries [5, 6]. The structures of these lignins differ significantly from that of native lignin. The major differences arise from cleavage of many of the ether linkages between the phenylpropanoid units that lowers the molar mass and increases the phenolic hydroxyl content of lignin. In most cases, these changes make the lignins much better suited for various applications such as adhesives [1, 7].

Further improvements in application performance can be achieved by modifications such as thermal post-treatment of kraft lignins by the CatLignin process [8, 9] that converts part of the G and S units to H units and catechol (Cat) units

✉ Chamseddine Guizani
chamseddine.guizani@vtt.fi

[1] VTT Technical Research Centre of Finland, P.O. Box 1000, 02044 VTT, Finland

Published online: 07 September 2023

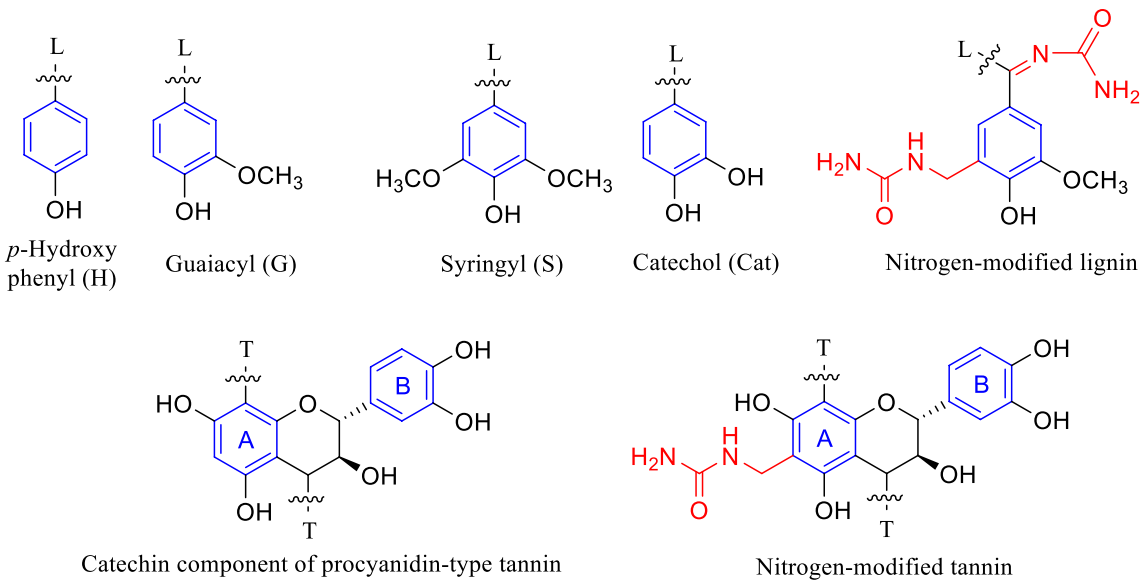

Fig. 1 Structural elements of technical lignins and condensed tannin and examples of their nitrogen derivatives

(Fig. 1). The lignins can also be chemically modified by introducing elements such as phosphorus and nitrogen in their structure with the aim of improving a particular functional property such as flame retardancy. Nitrogen modification is also a mean to introduce nitrogen functionalities into the surface of lignin derived carbon materials to enhance its electrochemical or adsorption performance [10–15]. An example of this strategy is nitrogen-modification via the Mannich and Schiff base reactions using, e.g., urea and formaldehyde [16, 17]. The Mannich reaction adds amino groups to the aromatic units and the Schiff base reaction may convert side chain carbonyl groups to imine groups (Fig. 1).

As for tannin [18, 19], it is found in many parts of trees but in most prominent species is mainly concentrated in the bark. The debarking of logs, usually the first step of wood processing, provides large quantities of bark that is mostly valorized in energy production. The two main types of tannin are hydrolyzable gallo- and ellagitannins and the flavonoid-based (condensed) tannins. Condensed tannins (Fig. 1) are found, e.g., in spruce and pine bark from which they can be isolated by alkali or hot-water extraction [20, 21]. The flavonoid units that make up the condensed tannins vary in structure, particularly in terms of the phenolic hydroxyl substituents on the aromatic A- and B-rings. For example, the procyanidin-type of condensed tannins found in Norway spruce bark [19] consist of catechin (Fig. 1) and its epimer, epicatechin. Tannins can be used for some of the same applications as technical lignins and similarly modified [22] to increase their nitrogen content (Fig. 1).

Lignins are promising precursors for a wide range of carbon materials [23, 24] including high-performance ACs for supercapacitor [25–27], adsorption [28], and catalysis [29] applications. Likewise, tannins represent untapped potential for engineering a wide variety of renewable materials [30] such as renewable ACs for energy storage in supercapacitors [31–36]. Nitrogen-modified polyphenols can be used to engineer nitrogen-doped biocarbons with enhanced properties in various applications related to catalysis and electrochemical energy storage [37].

The art and science of activated carbon (AC) engineering need to be constantly perfected to improve the control over their properties and performance. The current emerging AC applications related to gas and energy storage [38] are particularly demanding in terms of AC engineering, as the quality of the porosity, the nature of the defects, as well as the surface chemistry influence the AC performance [39–48].

High-surface-area ACs with hierarchical porosity can be synthesized from lignins and tannins using chemical activation methods [33, 49]. K_2CO_3 has been particularly effective for the synthesis of lignin-based [50–52] and tannin-based [53] ACs and has accordingly received a lot of attention. K_2CO_3 also has the major advantage of being a greener and safer chemical than KOH or $ZnCl_2$ [54].

To date, engineering of ACs from polyphenols using K_2CO_3 chemical activation has relied mainly on empirical approaches. For instance, the effects of polyphenolic precursor structure on its reactivity and its derived AC properties are little understood. Likewise, little is known about the effect of K_2CO_3/polyphenol ratio on the reactivity during carbonization. Some studies discuss the thermal behavior of lignins, tannins or other biomass components when mixed with K_2CO_3 but do not go deep enough into the details to derive quantitative information about

the reactivity as a function of the precursor properties or process parameters [49, 53, 55–57].

As the AC properties depend on the activation process parameters and burn-off level [58], controlling the carbon reactivity is a requisite for engineering high-performance ACs with controlled properties and optimized performance. Moreover, reactivity data are crucial for reactor design and activation process control [59, 60].

Studies on carbon reactivity during physical activation (also called thermal activation) are much more abundant than those on chemical activation [61]. Empirical approaches are more often the rule than the exception in many studies dealing with chemical activation of organic precursors [62]. Little is known on their reactivity as well as on the reaction mechanisms during chemical activation. Filling this gap is necessary to advance the art and science of AC engineering through chemical activation.

In this study, we addressed some of the aspects related to the thermal effects and kinetics of polyphenol chemical activation with K_2CO_3. In addition to our focus on the effects of process parameters (temperature and K_2CO_3/polyphenol ratio) on the precursor reactivity, we also investigated the effect of different lignin and tannin structures on the reactivity of their derived carbons towards K_2CO_3. Furthermore, we present the first simple kinetic model describing the reactivity of carbon surfaces from lignins and tannins during chemical activation with K_2CO_3.

2 Materials and methods

2.1 Materials

Softwood hydrolysis lignin (SW-HL) was obtained from St1 Cellunolix® plant (Kajaani, Finland) and softwood kraft lignin (SW-KL) from Domtar mill (North Carolina, USA). Softwood CatLignin (SW-CatL) was prepared from the SW-KL black liquor using the patented CatLignin technology involving thermal post-treatment of black liquor [8]. Industrial hardwood kraft lignin (HW-KL) was used as such or chemically modified (N-HW-KL) through the Mannich and Schiff base reactions to incorporate nitrogen into its structure [16]. Tannin was obtained by alkali-extraction of industrial spruce (*Picea abies*) bark with 24% NaOH for 90 min at 160ºC and recovered from the black liquor by acid precipitation, washing and drying [6]. It was used as such (SW-Tan) or after nitrogen-modification (N-SW-Tan) using the same protocol as for HW-KL [30]. K_2CO_3 was purchased from Merck.

2.2 Characterization of lignins and tannins

The lignins and tannins were characterized in terms of chemical and elemental composition, functional group content and molar mass distribution. Structural characterizations (whenever the samples were soluble) were performed using ^{31}P NMR and size-exclusion chromatography (SEC). Detailed descriptions of the analytical procedures and additional discussions about the results are given in the ESI (Table S1-S5).

2.3 Simultaneous thermal analysis coupled to mass spectrometry (STA-MS)

2.3.1 Experimental protocol

Carbonization and activation of lignins and tannins in mixtures with K_2CO_3 were studied using an analytical thermobalance (Netzsch Simultaneous Thermal Analyzer STA 449F1) coupled to a mass spectrometer. About 10 mg of each mixture was heated from room temperature up to 1000 °C at 10 °C/min under 70 mL of argon gas. The mass loss dynamics, heat flux and evolved gases were measured simultaneously. H_2O, CO and CO_2 gases were quantified after mass spectrometer (MS) calibration using CaC_2O_4. H_2O. More details about the MS calibration are given in the ESI (Figure S1 and Figure S2).

Different mixtures of lignins, tannins and K_2CO_3 were investigated (Table 1). The impregnation ratio (IR) – mass of K_2CO_3 over mass of lignin – was varied between 0.5 and 2 for the SW-HL and SW-KL lignins. The other samples were co-carbonized with K_2CO_3 at an IR of 1. Mixtures of polyphenols and K_2CO_3 were prepared by weighing using an analytical balance (precision of ± 0.01 mg) and thorough dry mixing using a pestle and a mortar. The total mass in a mixture was between 200 and 300 mg, out of which 10 ± 1 mg was transferred to the thermobalance crucible.

Table 1 Mixtures of lignins or tannins with K_2CO_3

Experiment	Sample	IR
SW-HL-IR0.5	Softwood hydrolysis lignin	0.5
SW-HL-IR1	Softwood hydrolysis lignin	1
SW-HL-IR2	Softwood hydrolysis lignin	2
SW-KL-IR0.5	Softwood kraft lignin	0.5
SW-KL-IR1	Softwood kraft lignin	1
SW-KL-IR2	Softwood kraft lignin	2
SW-CatL-IR1	Softwood CatLignin	1
HW-KL-IR1	Hardwood kraft lignin	1
N-HW-KL-IR1	Nitrogen-modified hardwood kraft lignin	1
SW-Tan-IR1	Softwood tannin	1
N-SW-Tan-IR1	Nitrogen-modified softwood tannin	1

3 Results and discussion

3.1 Direct carbonization of polyphenols

Direct polyphenol carbonization experiments were done to investigate their thermal reactivities in the absence of K_2CO_3. Although the samples showed significant differences in their mass loss dynamics (Figure S3 and Table S6), the char yields were surprisingly similar (in the range of 38–39 wt.%) except for the SW-CatL (~ 54 wt.%). The higher char yield and substantially lower mass loss peak for the SW-CatL can be explained by the removal of a major part of the phenylpropyl side chains during the black liquor thermal treatment [8, 9], which would have been otherwise removed during the carbonization step. The higher char yield might be also explained by the higher proportion of p-hydroxyphenyl and catechol units which undergo more readily dehydration, condensation, and charring reactions.

3.2 Effect of K_2CO_3 on the carbonization and activation of polyphenols

Thermograms of lignin and tannin samples mixed with K_2CO_3 (IR = 1) are shown in Fig. 2.

Regarding co-carbonization of lignins or tannins with K_2CO_3, remarkable differences were obtained between the thermograms that were measured (solid lines) and the ones that were calculated using a weighted sum of the polyphenol and K_2CO_3 thermograms (dashed lines). The thermogram of K_2CO_3 is shown in Figure S4 in the ESI. A major difference was observed at temperatures higher than ~ 600 °C due to the gasification of the carbonized polyphenols according to the global reaction:

$$K_2CO_3 + 2\,C \rightarrow 2K(s) + 3\,CO \quad (R1).$$

In addition, differences between the measured and weighted-sum thermograms were observed in the carbonization range due the catalytic effect of K_2CO_3, which is

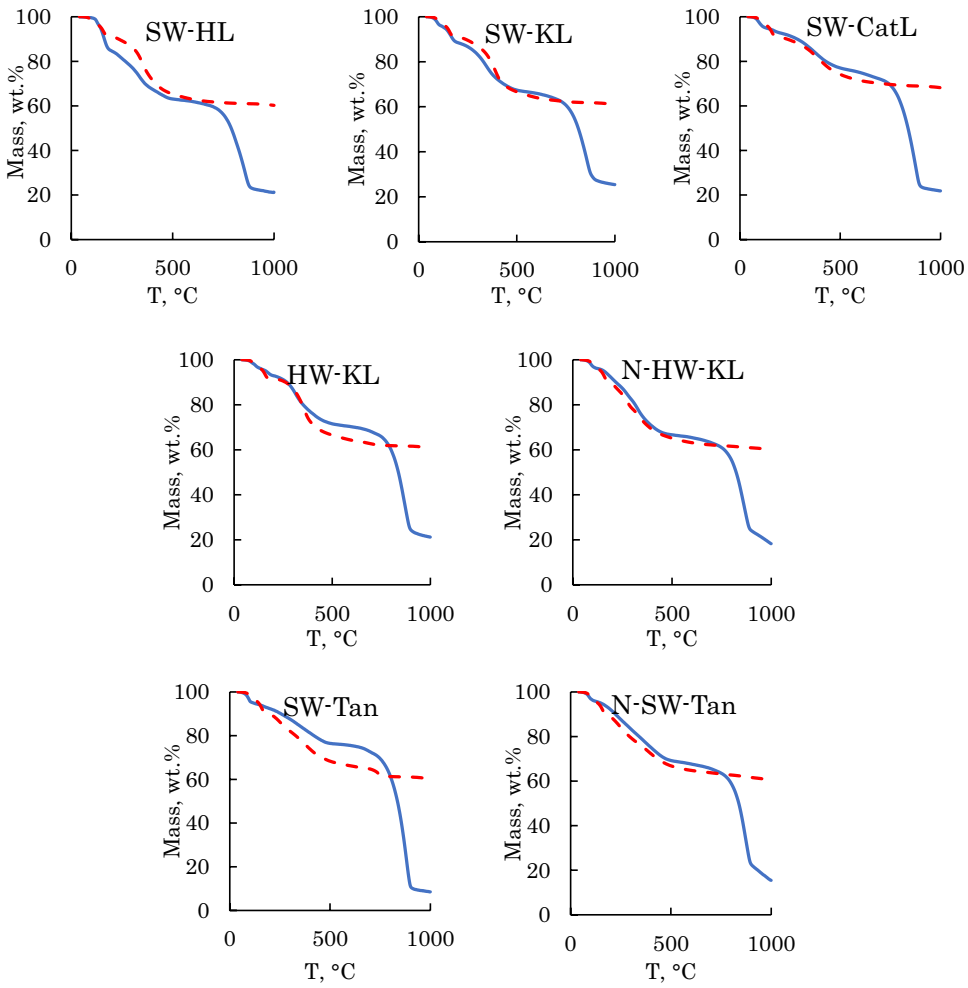

Fig. 2 Thermograms of polyphenol/K_2CO_3 mixtures at an IR of 1. The solid lines represent measured data and the dashes lines calculations from separate K_2CO_3 and polyphenol thermograms assuming a weighted sum (additivity)

known to act as a dehydration and charring catalyst during the carbonization of biopolymers [63–65].

The relative deviations in the carbonization and activation stages depend on the nature of the polyphenolic precursor. Difference curves are shown in the ESI (Figure S5). We calculated an empirical K_2CO_3 catalytic index during the carbonization stage (~ 200–600 °C) using the measured and weighted-sum thermograms according to the following equation:

$$CI = \frac{\sqrt{\sum_{Ti=200}^{Tn=600} (m_{Ti}^{mix} - m_{Ti}^{ws})^2}}{N} \quad (1)$$

- CI is the K_2CO_3 catalytic index during the carbonization stage.
- m_{Ti}^{mix} is the mass of the mixture at the temperature Ti.
- m_{Ti}^{ws} is the mass of the weighted sum at the temperature Ti.
- N is the number of observations.

A plot of the CI for the different samples is given in Figure S5.

The highest CI in the carbonization range was observed for SW-Tan, followed by SW-HL, while SW-KL and the modified lignins, SW-CatL and N-HW-KL, showed the lowest CI values. Owing to the marked structural differences and CI values between those samples, a possible hypothesis could be that the active sites during K_2CO_3 catalytic carbonization are the lignin side chains and the electron-rich carbons of the aromatic ring located *ortho* and *para* to the phenolic hydroxyls.

Indeed, the low CI for SW-KL compared to SW-HL can be explained by its highly condensed structure, which is attributed to the chemistry of the Kraft pulping process, involving complex cleavage and condensation reactions promoted by the hydroxyl and hydrogen sulfide ions. Those reactions ultimately modify the amount and distribution of lignin OH groups and can bond sulfur covalently to the Kraft lignin structure [66, 67].

As the reactions that SW-HL underwent during steam explosion are radically different from Kraft pulping [68], it would likely have more ether linkages, less carbon–carbon linkages, and less free phenolic groups compared to a SW-KL.

The higher CI observed for HW-KL compared to the SW-KL can be explained by the higher proportion of syringyl units in hardwood lignins, which leads to less condensed structure during kraft pulping [69]. In addition, the HW-KL has lower sulfur amount (1.7 wt.%) compared to the SW-KL (2.2 wt.%), which can also reduce the K_2CO_3 catalytic activity when covalently bond to an active site in the aromatic sidechains.

In the production of SW-CatL, the side chains are largely cleaved during the heat treatment [70], which reduces the number of active sites and might explain the low catalytic action of K_2CO_3.

In the case of N-modified HW-KL, nitrogen modifications may have occurred at both the unsubstituted aromatic carbons *ortho* to phenolic hydroxyls and side chain carbonyl groups [71]. A limited availability of these sites after chemical modification may explain the lower CI for the N-HW-KL. It should be noted, however, that the aliphatic substituents introduced via the Mannich reaction "dilute" the aromatic content. If aromatic rings are associated with higher CI, this modification can also reduce CI on a mass basis.

The spruce SW-Tan sample has predominantly procyanidin-type condensed tannin structures [19, 72]. K_2CO_3 showed the highest catalytic activity during carbonization with this sample (CI = 9.1). Conversely, its catalytic action during the co-carbonization with the nitrogen-modified N-SW-Tan was much less pronounced (CI = 3.9). This reduction of the catalytic activity can also be related to fewer electron-rich carbons located *ortho* or *para* to the phenolic hydroxyls being available after the nitrogen modification [71].

The catalytic effect of K_2CO_3 during co-carbonization with polyphenols was also visible in the heat flux DSC curves, which changed markedly compared to the pure samples due to the change in the carbonization chemistry and associated thermal effects (Figures S3 and S6). Altogether, these observations indicate that K_2CO_3 interacted with lignin during the heat treatment and catalyzed its carbonization reactions at sub gasification temperatures [73].

Interestingly, although the char yield during carbonization was almost similar for all original samples except for SW-CatL, the yield of residual solids varied much more after co-carbonization with K_2CO_3. This result suggests that the reactivity of the carbonized polyphenols during the activation stage might depend on the polyphenol structural properties. A discussion on the structural-thermal reactivity relationship is given in the next section.

3.3 Polyphenol structure-thermal reactivity relationships

Lignins and tannins that could be dissolved and analyzed through SEC and ^{31}P NMR, showed remarkable structure-thermal reactivity relationships during the chemical activation with K_2CO_3 (Fig. 3).

For the unmodified polyphenols, the K_2CO_3 CI of the carbonization stage decreased with the total (aliphatic + phenolic) number of OH groups following a quadratic trend. In addition, the yield of solid residue (mixture of activated carbon and unreacted K_2CO_3) after activation increased linearly with the total number of OH groups.

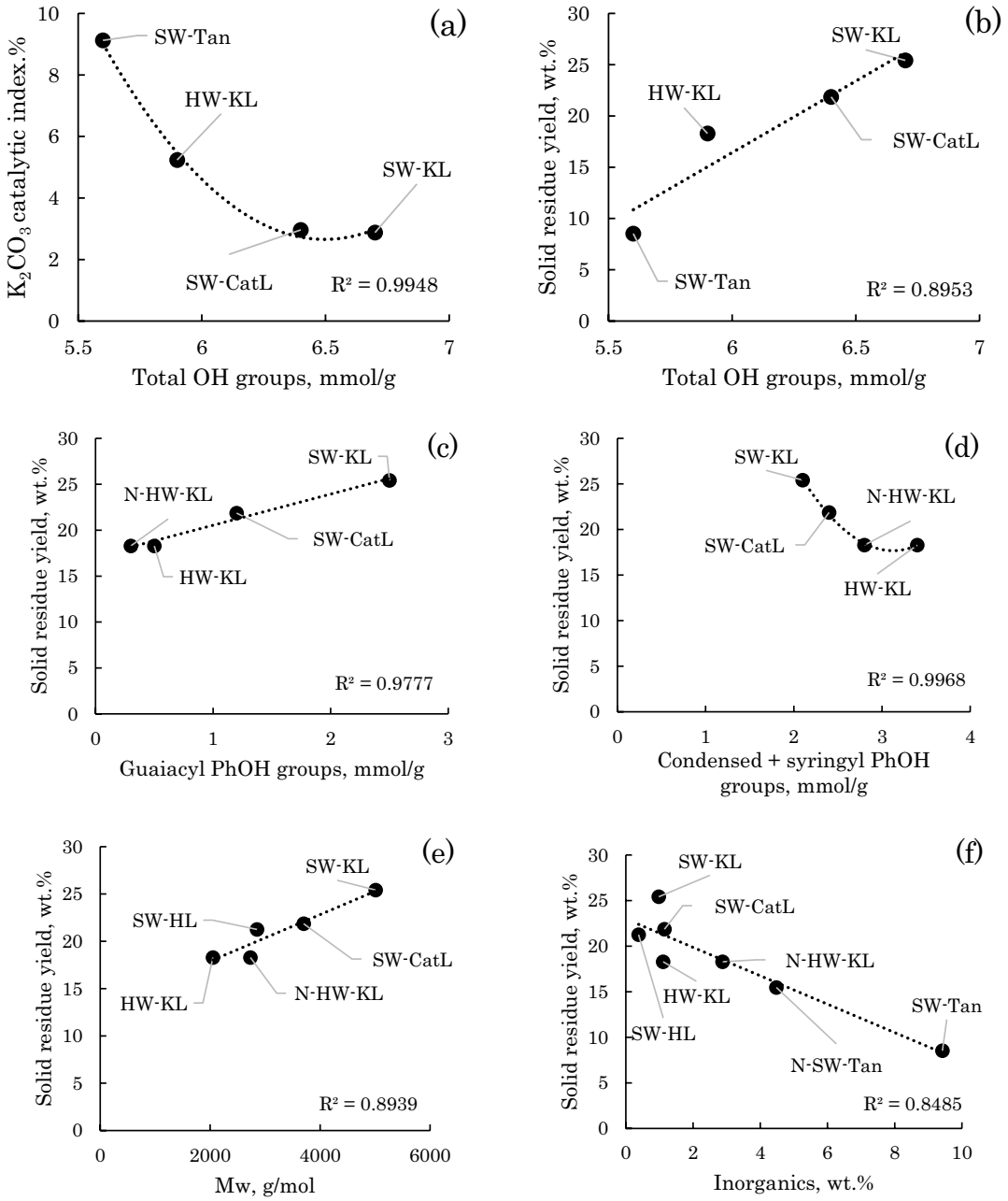

Fig. 3 Remarkable relationships between reactivity and structural properties of polyphenols during chemical activation with K_2CO_3

These observations suggest that the samples which had the lowest catalytic activity with K_2CO_3 during carbonization reacted the least during the activation stage. Hence, the activation stage seems to depend on the reactions that occur during the carbonization stage between the carbonizing polyphenol and K_2CO_3. A possible explanation of the mass increase during TGA can be related to the ability of K_2CO_3 to deprotonate the moderately acidic phenolic hydroxyls of phenols (pKa ~ 10) which could enhance the crosslinking and favor the formation of a solid carbon phase during the heat treatment. Such crosslinked carbonized structures might be less reactive and limit the formation of C(O) surface complexes during the gasification stage.

The solid residue yield increased with the content of guaiacyl-type phenolic groups and decreased with the sum of condensed (= with carbon-substituted *ortho* position) and syringyl-type OH groups (including the modified N-HW-KL sample). These findings support the hypothesis that the electron-rich carbons of the aromatic ring located *ortho* and *para* to the phenolic hydroxyls are the main active sites during K_2CO_3 catalytic carbonization.

For all the lignin samples tested, the yield of solid residue after activation increased with their weight-average molecular weight (Mw). Here again, it is quite remarkable that such a trend was not observed during direct carbonization of the polyphenol samples. SW-KL had the highest Mw and was the least reactive, while HW-KL had the lowest Mw and was the most reactive.

Lower molar mass lignins were therefore more reactive than higher molar mass ones during the activation with K_2CO_3. Obtaining reactive low molar mass lignins would be possible following simple and scalabe solvent fractionation methods [74, 75].

The solid residue yield was also correlated to the content of inorganics in the polyphenols, which is remarkabely different from the direct carbonization experiments wherein the char yields were nearly identical except for the SW-CatL (Table S6). This result suggests that inorganics present initially in the polyphenol structure play a major role during the catalytic carbonization and activation with K_2CO_3. The presence of K_2CO_3 seems necessary to trigger their catalytic action. The operating mechanisms are however unclear and will need further research that goes beyond the scope of the present study.

All in all, the above-mentioned structure-thermal reactivity correlations imply that engineering the structure of polyphenols would also lead to modifications in burnoff levels, and consequently in the AC properties without additional process energetic (temperature) and material (K_2CO_3) expenses.

3.4 Effect of K_2CO_3/lignin ratio on the carbonization and activation of lignins: case of SW-HL and SW-KL

The effect of K_2CO_3/lignin ratio was investigated for SW-HL and SW-KL. Thermograms of SW-HL and SW-KL mixed with K_2CO_3 at different IR are shown in Fig. 4.

The deviations between the measured thermograms (solid lines) and the ones calculated using a weighted sum of the lignin and K_2CO_3 thermograms (dashed lines) increased with an increase in IR during both the carbonization and the activation stages. These differences can be attributed to the increasing catalytic activity of K_2CO_3 during the carbonization stage and to the higher burn-off level during the activation. The related DTG plots are shown in Figure S7.

The mass loss rate decreased in the carbonization range (~ 200–600 °C) as the IR increased due to the lower amount of lignin in the mixtures. In addition, we observed a shift of the carbonization peak to lower temperatures for both lignins. These observations were corroborated by the heat flux profiles, which changed markedly compared to the case of pure lignin. DSC heat fluxes of SW-HL and SW-HL/K_2CO_3 mixtures (Fig. 5) illustrate well these thermal changes.

The exothermic peak not only decreased with the IR, but also shifted to lower temperatures. In addition, a new endothermic peak appeared at ~ 500 °C. This new endothermic peak was observed for all samples and IR and might be associated with the formation of K_2O and C(O) surface complexes upon the reaction of K_2CO_3 with the polyphenol during carbonization [76].

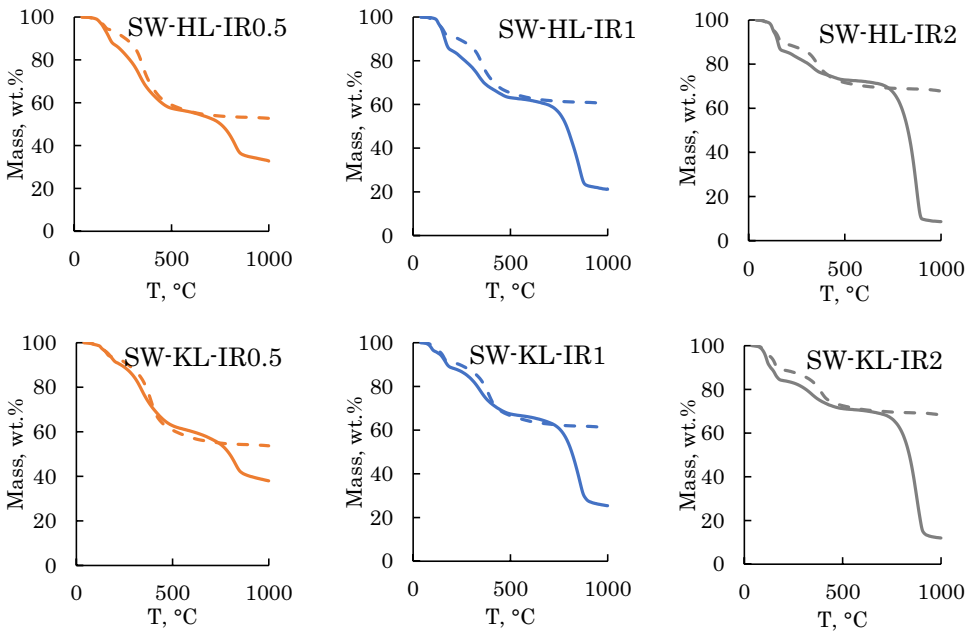

Fig. 4 Thermograms of SW-HL/K_2CO_3 and SW-KL/K_2CO_3 mixtures at different IR. The solid lines represent the measured data, and the dashes lines the weighted sum calculations from separate K_2CO_3 and lignin thermograms (additivity)

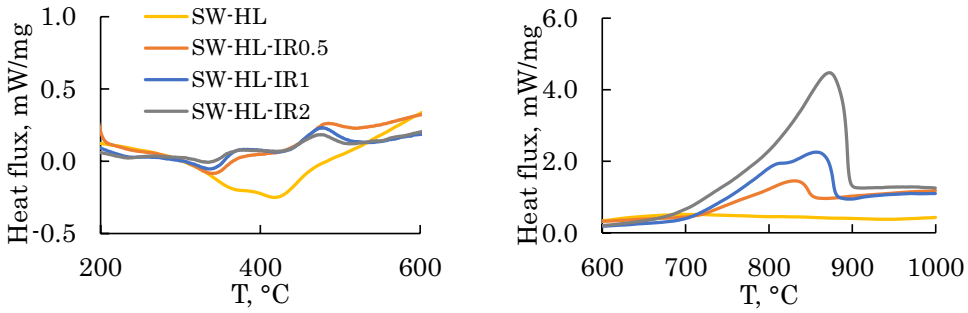

Fig. 5 DSC heat flux traces of SW-HL and SW-HL/K_2CO_3 mixtures at different IR

The thermograms indicate that the activation onset temperature was in the range of ~ 650–700 °C. The activation mass loss peak increased with the IR as did the heat flux DSC peak, indicating a higher degree of progress of the activation reaction. The final mass decreased consequently due to higher carbon conversion levels. In addition, the thermograms indicate a shift of the mass loss peak to higher temperatures during the activation as the IR increased (see Figure S8). The origin of this shift is not clear. It might be due to the endothermic effects during the gasification reaction, which cool down the sample locally and consequently cause a shift in the observed mass loss peak. Another explanation could be related to an inhibition of C(O) surface group decomposition by a higher amount of CO gas molecules formed in their vicinity (at higher IR), and which would therefore slow down their decomposition kinetics according to the Langmuir–Hinshelwood theory [77].

During the activation stage, only CO could be detected via mass spectrometry according to the global reaction:

$$K_2CO_3 + 2\,C \rightarrow 2\,K(s) + 3\,CO \quad (R1)$$

The CO emission profile was superimposable on the DTG peak profile in the activation stage (see Fig. 6). After calibration of the mass spectrometer with $CaC_2O_4.H_2O$, the CO released during the activation could be quantified (see Fig. 6).

For both lignins we observed linear correlations between the IR and several of the parameters determined from the STA-MS analysis, as illustrated in Fig. 6. The CO amount was proportional to the IR. The mass loss rate peak and

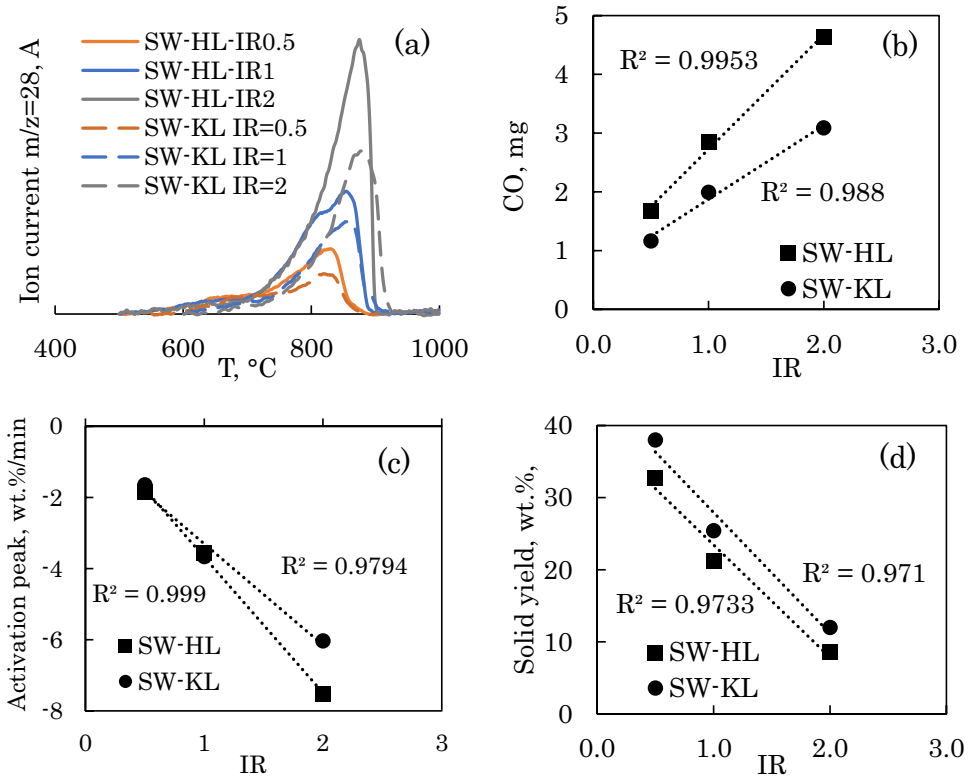

Fig. 6 **a** Example of CO emission profiles during the carbonization of HL/K_2CO_3 and KL/K_2CO_3 mixtures (IR = 1). **b** Quantity of CO emitted during the activation stage as a function of the IR. **c** Maximum mass loss rate as a function of IR during the activation stage. **d** Solid yield as a function of IR

the residual solid amount (mixture of activated carbons and residual K_2CO_3) were also both linearly correlated with the IR.

It is important to note that increasing the IR further to 4 in the case of SW-HL did not result in a proportional decrease of the final mass. The amount of CO produced and the mass loss during activation were even lower than the values obtained at IR = 2. This result indicates that the observed linarity is valid only within a certain range of lignin/K_2CO_3 ratios and that high IR ratios during chemical activation, unlike often reported in the literature, are not needed.

Hydrolysis lignin showed overall a higher reactivity towards K_2CO_3 as shown by the systematically lower residue yield and the higher CO amount at the different IR. Due to fundamental isolation and recovery process differences, kraft and hydrolysis lignins differ chemically and structurally. Typically, hydrolysis lignin residue has notably high content of residual cellulose compared to other types of technical lignin. Hydrolysis lignin is more native-like lignin than kraft lignin, whose structure is significantly altered during the pulping process [78]. In addition, the sulfur content in hydrolysis lignin is lower compared to that on kraft lignin, while the hydrolysis lignin contains some nitrogen due to the enzyme residues from the hydrolysis step [79]. Those fundamental chemical and structural differences are likely at the origin of the observed differences in reactivity.

3.5 Modeling the activation reaction kinetics

3.5.1 Phenomenology of carbon-K_2CO_3 activation reactions and model hypotheses

Kinetic models describing the gasification of carbons during physical activation have been extensively developed to predict and control the burn-off of carbons in activation reactors and gasifiers [80–82]. Conversely, there is a striking lack of information on the kinetics of carbon surface gasification during chemical activation. To the authors' best knowledge, there are no published studies about the kinetics of carbon surface gasification during chemical activation with K_2CO_3, although they are crucial for reactor design and reactivity control. In this section, we present a simple model that can describe the gasification of carbon surfaces during K_2CO_3 chemical activation of polyphenols.

Based on the present thermo-analytical study as well as several literature reports, we can assume that the activation stage can be well described as follows:

- At temperatures of ~ 600-700 °C, the carbon formed during the co-carbonization of polyphenol/K_2CO_3 starts to gasify into CO as shown by the mass spectrometry measurements according to the global reaction:

$$K_2CO_3 + 2\,C \rightarrow 2\,K(s) + 3\,CO \quad (R1)$$

- This global reaction can be assumed to occur in two consecutive steps involving the formation of K_2O, K and C(O) surface complexes. During the first step, K_2CO_3 reacts with the polyphenol to form K_2O and C(O) surface complexes, according to the reaction (R2) [76, 83, 84]:

$$K_2CO_3 + C \rightarrow K_2O + 2\,C(O) \quad (R2)$$

- In the second step, K_2O reacts with the carbonized polyphenol to form metallic potassium and C(O) surface complexes according to the reaction (R3).

$$K_2O + C \rightarrow 2\,K + C(O) \quad (R3)$$

- The C(O) surface complexes formed via reactions (R2) and (R3) decompose into CO, leading to the observed mass loss. The reaction can be described as:

$$C(O) \rightarrow CO \quad (R4)$$

The decomposition of C(O) surface complexes is the rate-limiting step which controls the overall rate of mass loss. It is common to all gasification reactions with O_2, CO_2, and H_2O [85]. Our main hypothesis in the following modeling strategy is that it is also the rate-limiting step during K_2CO_3 chemical activation of carbonized polyphenols. In addition to this simplified reaction phenomenology, we consider the following additional hypotheses for the kinetic modeling:

- The activation stage corresponds to the decomposition of C(O) surface complexes into CO gas following (R4).
- The rate of CO formation (or mass loss rate) depends on the unreacted fraction of C(O) surface complexes.
- The decomposition of C(O) surface complexes follows the Arrhenius law.
- The C(O) surface complexes are energetically equivalent.
- The reaction occurs in the chemical domain; There are no mass transfer limitations or re-adsorption of CO on the reacting carbon surface; The CO molecules leave the reaction zone immediately after being formed.

With this simplified picture of the carbon surface gasification, the reaction conversion rate can be written as a product of a reaction rate constant (which depends on temperature according to the Arrhenius law) and a conversion function $f(\alpha)$:

$$\frac{d\alpha}{dt} = k(T)f(\alpha)$$

$k(T)$ is the reaction rate constant which can be expressed by the Arrhenius law:

$$k(T) = Ae^{\frac{-E_a}{RT}}$$

E_a is the activation energy, A is the pre-exponential factor, and n is the reaction order.

$f(\alpha)$ can take several forms which depend on the decomposition mechanism [86].

The linear form of the rate equation reads:

$$Ln\left(\frac{1}{f(\alpha)}\frac{d\alpha}{dt}\right) = A - \frac{E_a}{R}\frac{1}{T}$$

A plot of $Ln\left(\frac{1}{f(\alpha)}\frac{d\alpha}{dt}\right)$ as a function of $\frac{1}{T}$ should result in a straight line provided that $f(\alpha)$ is the right conversion function that describes the decomposition of C(O) surface complexes. The Arrhenius parameters can be then easily identified by applying a linear regression.

Conversion profiles can be obtained from the CO emission profiles, the mass loss profiles, or the DSC profiles in the activation region (T ~ 600–1000 °C), considering the ~ 600 °C as the onset of the activation (see Figure S9). Examples of conversion profiles calculated from the CO emission profiles for the SW-HL and SW-KL in different mixtures with K_2CO_3 are shown in Fig. 7.

Among the different models we tested [86], the contracting sphere model, $f(\alpha) = 3(1-\alpha)^{2/3}$, led systematically to the best fit, regardless of the sample type, the impregnation ratio or the data used for the calculations. Example linearized rate plots for SW-HL and SW-KL in different mixtures with K_2CO_3 are shown in the same figure.

The modeling was successful for IR = 1 and IR = 2, but less satisfactory for the IR = 0.5 experiments. In addition to being shifted at low temperatures, the conversion profiles at the lowest IR had a slightly different shape compared to higher IR and showed a faster conversion rate at lower conversion levels (α < 0.3). The reasons for the temperature shift (see Figure S8) are not fully clear, but we suspect that local sample cooling due to the highly endothermic character of the activation reactions, in addition to melting of unreacted K_2CO_3, might have caused it. Heat and mass transport limitations, as well as re-adsorption of CO on the carbon surface might have slowed down the decomposition reaction rate and caused the observed temperature shift. Finally, the reactivity of the carbon surface might also depend on the carbon surface coverage, which changes with the IR.

As a result, the identified kinetic parameters varied with the IR. We observed a kinetic compensation effect for which a change in the apparent activation energy was compensated by a change in the pre-exponential factor (Fig. 8). Changes in carbon surface reactivity might have contributed to the observed compensation, but the effects of heat and mass transport limitations, endothermicity and sample cooling cannot be ruled out. Statistical compensation effects may

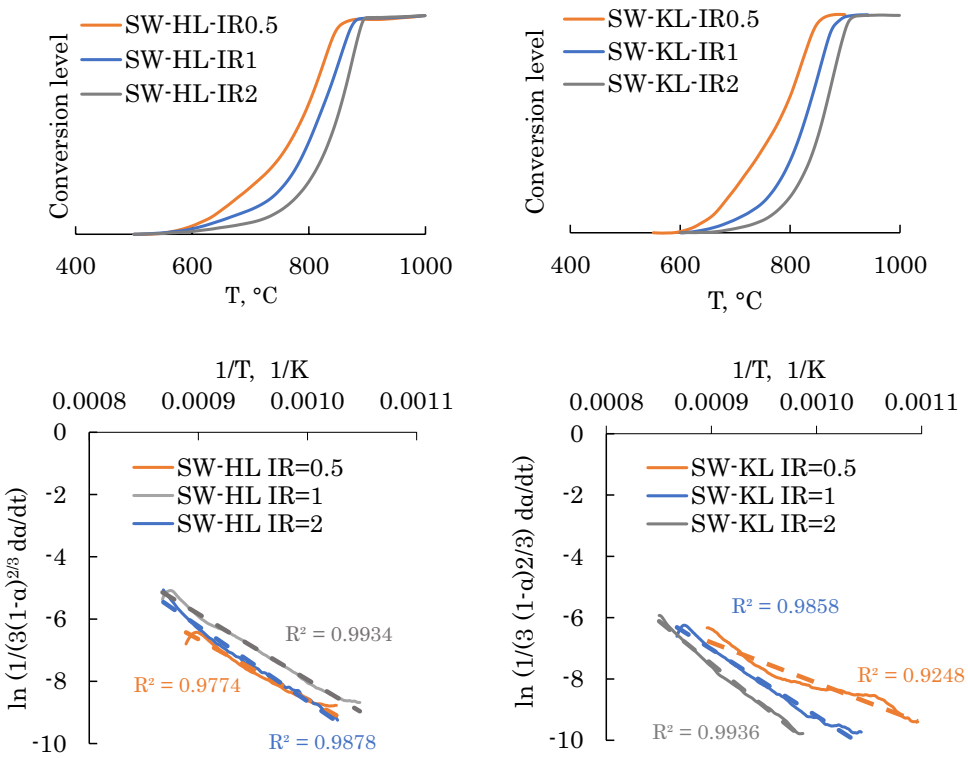

Fig. 7 Top figures are the activation stage conversion plots for SW-HL/K_2CO_3 mixtures (left) and SW-KL/K_2CO_3 mixtures (right). The conversion plots were calculated from the CO profiles. Bottom figures are the linearized rate plots of SW-HL/K_2CO_3 mixtures (left) and SW-KL/K_2CO_3 mixtures (right) during the activation stage. $f(\alpha)$ is defined by the contracting sphere model

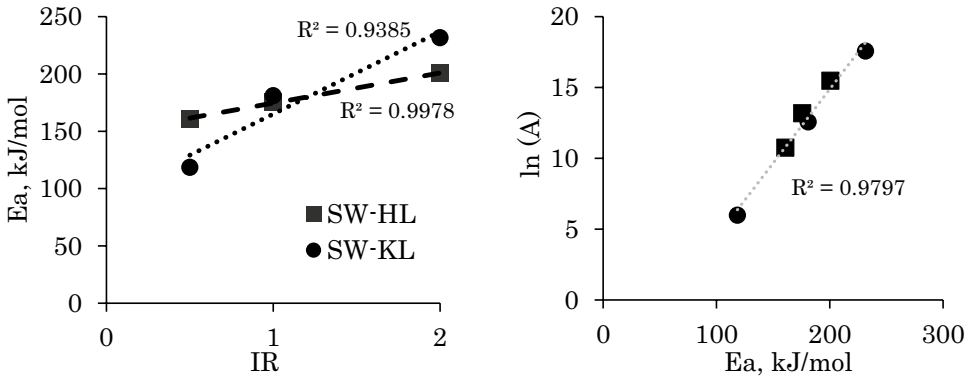

Fig. 8 (left) Activation energy of carbon gasification during the activation stage as a function of IR for SW-HL/K_2CO_3 mixtures and SW-KL/K_2CO_3 mixtures. (right) Compensation plot showing the linearity between ln(A) and Ea. The data were calculated from the CO conversion profiles

be indeed caused solely by errors in measuring temperatures and not by a physiochemical property of the sample [87–90].

Fitting the model to conversion profiles calculated from the mass data in the activation range yielded results close to the ones obtained from CO gas conversion profiles. However, fitting the model to conversion profiles from DSC curves led to different E and A values, and to different trends of E as a function of IR (Figure S10 and Figure S11). The E values obtained from DSC profiles showed less dependence on the IR. This difference might be related to the baseline definition and subtraction in the DSC data, as well as to shifts of the DSC signal in relation to the CO and mass loss profile in the activation stage. The thermocouple and microbalance response times and sensitivities might have been different, causing shifts and differences in the conversion profiles. A plate-style heat flux DSC detector, such the one we used, sacrifices sensitivity and quick response in favor of contact repeatability to enable the quantification of total heat flow after calibration with known standards [91].

The fact that CO and mass conversion profiles are based on sample mass loss (mass and gas measurement), while the DSC profile is based on temperature measurements, can explain the observed differences in conversion profiles as a function of temperature. Furthermore, the DSC signal might also include thermal effects which are not caused by the activation reaction, such as melting of unreacted K_2CO_3. These issues need to be further clarified. The identified kinetic parameters and fit quality coefficients are given in Table S7.

3.6 Is this the solid-state decomposition model applicable to all polyphenolic carbon surfaces?

The same model was extended to the other polyphenol/K_2CO_3 mixtures (IR = 1). The model was tested using conversion profiles calculated from mass and DSC data. The linearized rate plots and the identified kinetic parameters during the activation stage are shown in Fig. 9. The model was remarkably well applicable to all polyphenol/K_2CO_3 mixtures. Kinetic and fitting quality parameters for all the samples are given in Table S7.

The kinetic parameters varied as a function of the polyphenol sample and conversion profile origin. The identified activation energy of polyphenol carbon surface activation with K_2CO_3 lay between 180–270 kJ/mol, close to the range of E values reported in the literature for physical activation of carbon surfaces using CO_2 or H_2O [81, 92–95]. This similarity of *E* values for physical and chemical activation methods can be rationalized by the formation of C(O) surface complexes, which is the common rate-limiting step of carbon surface gasification reactions [85, 96].

Variation in the kinetic parameters can be explained by different carbon surface reactivities, which depend on the polyphenol structure as discussed in the previous section. The number of active sites and the extent of surface coverage by intermediate C(O) complexes during the activation stage can vary with the polyphenol type. But here again, pseudo-compensation effects caused by experimental inaccuracies or arising from conversion profiles cannot be ruled out for the same reasons we discussed above (see Figure S12).

Marsh and Rodríguez-Reinoso have also established the existence of a compensation effect during gasification of carbon surfaces: "*it is not possible to enhance the rate by lowering the activation energy and at the same time increasing the rate constant k*(*T*)". These considerations seem to apply to all gasification reactions of oxygen, carbon dioxide, steam and oxides of nitrogen [60], as well as to chemical activation by K_2CO_3 as in the present case.

4 Conclusions

The present study revealed several new findings related to the chemical activation of lignins and tannins using K_2CO_3:

- It was shown, for the first time, that the reactivity of lignins and tannins during chemical activation with K_2CO_3 depends remarkably on content in inorganics, their molecular weight and their OH functionalities.
- The catalytic effect of K_2CO_3 during the carbonization stage decreased with the total (aliphatic + phenolic)

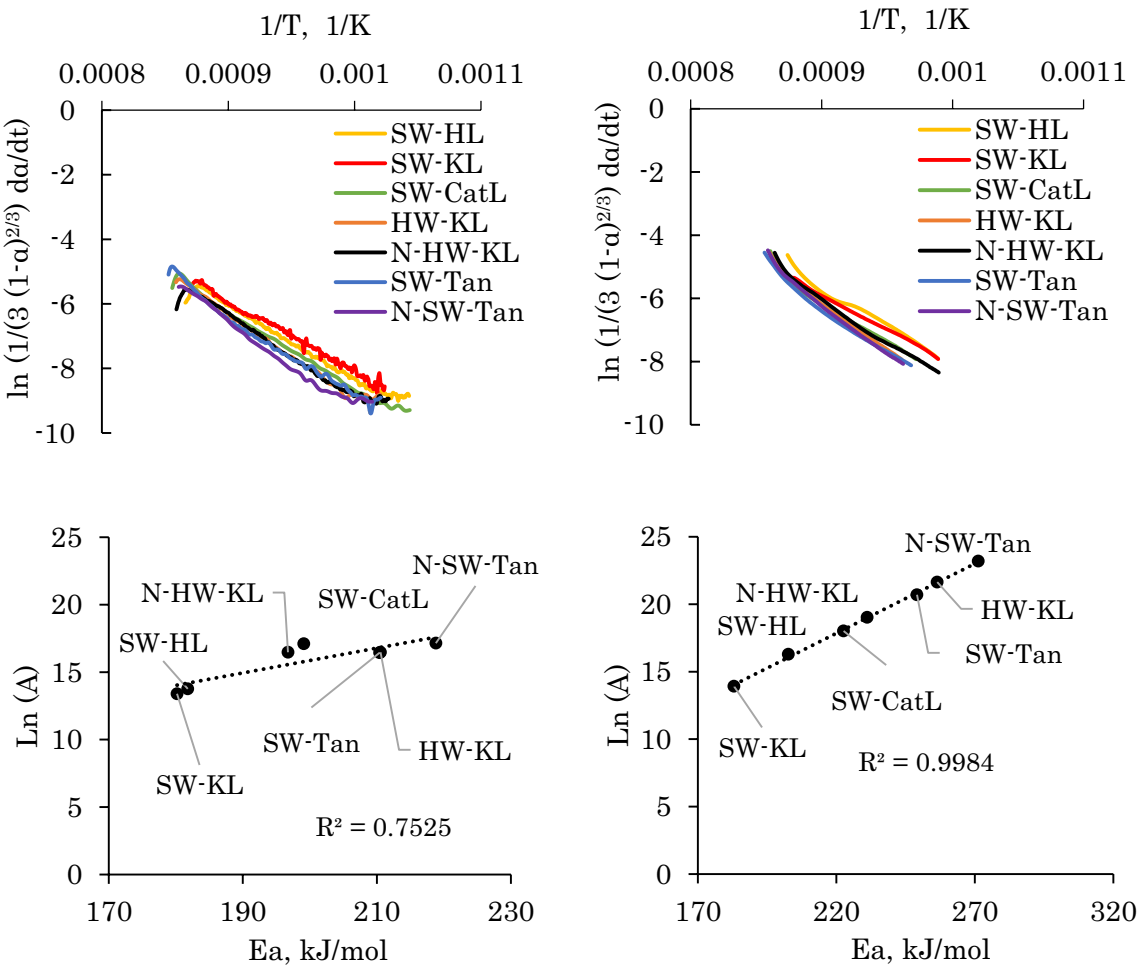

Fig. 9 (Top) Linearized rate plots for the different polyphenol/K_2CO_3 mixtures (IR = 1) during the carbon surface activation stage. (Bottom) Compensation plot showing pre-exponential factors as a function of activation energy for the different polyphenols. The plots on the left-hand side were obtained from mass loss conversion profiles. The plots on the right-hand side were obtained from DSC conversion profiles

number of OH groups following a quadratic trend. The yield of solid residue (mixture of activated carbon and unreacted K_2CO_3) after activation increased linearly with the total number of OH groups and average molecular weight, and decreased with the inorganics content.

- The combined structural and thermal analyses support the hypothesis that the electron-rich carbons of the aromatic ring located *ortho* and *para* to the phenolic hydroxyls are the main active sites during K_2CO_3 catalytic carbonization and activation.
- Inorganics which are initially present in the polyphenol structure have a substantial effect on the solid residue yield after K_2CO_3 catalytic carbonization and activation, but surprisingly not during direct carbonization. Their catalytic effect is triggered by the presence of K_2CO_3.
- Using structurally different softwood kraft and hydrolysis lignins, it was shown that the activation burn-off level depends linearly on the IR in the range of 0.5–2. The final BO level depends, however, on the precursor structural properties.
- Increasing the IR further to 4 did not result in a proportional decrease of the BO level. This implies that using a high IR, as is often the case in the literature, is not needed.
- We developed the first kinetic model describing the K_2CO_3 activation of carbon surfaces from lignins and tannins. The model was applicable to all the samples and IR we investigated.
- The model is based on the solid-state decomposition kinetics and assumes that the rate-limiting step governing the mass loss during the activation corresponds to the thermal decomposition of C(O) surface complexes, which were formed through a reaction of K_2CO_3 with the lignin at sub-gasification temperatures.
- The identified activation energies lay in the range of values reported for heterogenous carbon gasification reac-

tions with O_2, H_2O, or CO_2, in which the decomposition of C(O) surface complexes is also the common and rate-limiting step.
- Kinetic compensation effects were observed when varying the sample, the IR or the raw data used for model fitting. Variations in the Arrhenius kinetic parameters were ascribed to differences in carbon surface properties as well as to experimental errors.

The new findings lay the ground for a more systematic engineering of ACs from renewable polyphenols using a greener K_2CO_3 chemical activation route. The methodology we presented can be applied to other chemical activation routes to get better insights into the underlying mechanisms and a better control over the AC properties in the emerging energy and gas storage applications. Future work will focus on disclosing relationship between polyphenol structure and the multiscale properties of ACs obtained by K_2CO_3 chemical activation.

Supplementary Information The online version contains supplementary material available at https://doi.org/10.1007/s42823-023-00601-4.

Authors contribution The authors confirm contribution to the paper as follows: Conceptualization: Chamseddine Guizani; data collection: Chamseddine Guizani, Petri Widsten, Riina Paalijärvi, Antti Pasanen, Jonathan Berg; analysis and interpretation of results: Chamseddine Guizani, Petri Widsten; Writing—Original Draft: Chamseddine Guizani, Petri Widsten. Writing—Review & Editing: All authors. Supervision and project administration: Chamseddine Guizani, Katariina Torvinen. All authors reviewed the results and approved the final version of the manuscript.

Funding Open Access funding provided by Technical Research Centre of Finland (VTT).

Data availability The data will be available from the corresponding author upon a reasonable request.

Declarations

Conflict of interests On behalf of all authors, the corresponding author states that there is no conflict of interest.

References

1. Norgren M, Edlund H (2014) Lignin: recent advances and emerging applications. Curr Opin Colloid Interface Sci. https://doi.org/10.1016/j.cocis.2014.08.004
2. Tomani P (2010) The lignoboost process. Cellul Chem Technol 44:53–58
3. Kouisni L, Holt-Hindle P, Maki K, Paleologou M (2014) The LignoForce System™: A new process for the production of high-quality lignin from black liquor. Pulp and Paper Canada 115:18–22
4. A.J. Ragauskas, G.T. Beckham, M.J. Biddy, R. Chandra, F. Chen, M.F. Davis, B.H. Davison, R.A. Dixon, P. Gilna, M. Keller, P. Langan, A.K. Naskar, J.N. Saddler, T.J. Tschaplinski, G.A. Tuskan, C.E. Wyman (2014) Lignin valorization: Improving lignin processing in the biorefinery. Science (1979). doi:https://doi.org/10.1126/science.1246843.
5. Balakshin MY, Capanema EA, Sulaeva I, Schlee P, Huang Z, Feng M, Borghei M, Rojas OJ, Potthast A, Rosenau T (2020) New Opportunities in the Valorization of Technical Lignins. Chemsuschem. https://doi.org/10.1002/cssc.202002553
6. M. Borrega, A. Kalliola, M. Määttänen, A.S. Borisova, A. Mikkelson, T. Tamminen (2022) Alkaline extraction of polyphenols for valorization of industrial spruce bark, Bioresour Technol Rep. 19 : 101129. doi:https://doi.org/10.1016/J.BITEB.2022.101129.
7. Kai D, Tan MJ, Chee PL, Chua YK, Yap YL, Loh XJ (2016) Towards lignin-based functional materials in a sustainable world. Green Chem 18:1175–1200. https://doi.org/10.1039/c5gc02616d
8. H. Wikberg, T. Ohra-aho, J. Leppävuori, T. Liitiä, H. Kanerva (2018) Method for producing reactive lignin
9. Widsten P, Tamminen T, Liitiä T (2020) Natural Sunscreens Based on Nanoparticles of Modified Kraft Lignin (CatLignin). ACS Omega 5:13438–13446. https://doi.org/10.1021/acsomega.0c01742
10. Treeweranuwat P, Boonyoung P, Chareonpanich M, Nueangnoraj K (2020) Role of Nitrogen on the Porosity, Surface, and Electrochemical Characteristics of Activated Carbon, ACS. Omega. https://doi.org/10.1021/acsomega.9b03586
11. Zheng L, Wang X, Wang H, Zhao X, Kong F, Liu Y (2022) Novel Nitrogen-Doped Porous Carbon with High Surface Areas Prepared from Industrial Alkali Lignin for Supercapacitors. ChemElectroChem. https://doi.org/10.1002/celc.202200869
12. G. Lota, B. Grzyb, H. Machnikowska, J. Machnikowski, E. Frackowiak (2005) Effect of nitrogen in carbon electrode on the supercapacitor performance, Chem Phys Lett. 404. doi:https://doi.org/10.1016/j.cplett.2005.01.074.
13. Chen J, Yang J, Hu G, Hu X, Li Z, Shen S, Radosz M, Fan M (2016) Enhanced CO2Capture Capacity of Nitrogen-Doped Biomass-Derived Porous Carbons. ACS Sustain Chem Eng 4:1439–1445. https://doi.org/10.1021/acssuschemeng.5b01425
14. J. He, J. To, J. Mei, Z. Bao, J. Wilcox (2014) Facile synthesis of nitrogen-doped porous carbon for selective CO2 capture, In: Energy Procedia, Elsevier Ltd, p. 2144–2151. doi:https://doi.org/10.1016/j.egypro.2014.11.233.
15. C. Zhang, W. Song, G. Sun, L. Xie, J. Wang, K. Li, C. Sun, H. Liu, C.E. Snape, T. Drage (2013) CO_2 capture with activated carbon grafted by nitrogenous functional groups. Energy and Fuels p. 4818–4823. doi:https://doi.org/10.1021/ef400499k.
16. Zhang R, Xiao X, Tai Q, Huang H, Hu Y (2012) Modification of lignin and its application as char agent in intumescent flame-retardant poly(lactic acid). Polym Eng Sci 52:2620–2626. https://doi.org/10.1002/pen.23214
17. Widsten P, Tamminen T, Paajanen A, Hakkarainen T, Liitiä T (2020) Modified and unmodified technical lignins as flame

retardants for polypropylene. Holzforschung. https://doi.org/10.1515/hf-2020-0147
18. Pizzi A (2019) Tannins: Prospectives and actual industrial applications. Biomolecules. https://doi.org/10.3390/biom9080344
19. Bianchi S, Kroslakova I, Janzon R, Mayer I, Saake B, Pichelin F (2015) Characterization of condensed tannins and carbohydrates in hot water bark extracts of European softwood species. Phytochemistry 120:53–61. https://doi.org/10.1016/j.phytochem.2015.10.006
20. Borrega M, Kalliola A, Määttänen M, Borisova AS, Mikkelson A, Tamminen T (2022) Alkaline extraction of polyphenols for valorization of industrial spruce bark. Bioresour Technol Rep. https://doi.org/10.1016/j.biteb.2022.101129
21. Kemppainen K, Siika-aho M, Pattathil S, Giovando S, Kruus K (2014) Spruce bark as an industrial source of condensed tannins and non-cellulosic sugars. Ind Crops Prod 52:158–168. https://doi.org/10.1016/j.indcrop.2013.10.009
22. Pöhler T, Widsten P, Hakkarainen T (2022) Improved Fire Retardancy of Cellulose Fibres via Deposition of Nitrogen-Modified Biopolyphenols. Molecules. https://doi.org/10.3390/molecules27123741
23. Chatterjee S, Saito T (2015) Lignin-Derived Advanced Carbon Materials. Chemsuschem 8:3941–3958. https://doi.org/10.1002/cssc.201500692
24. Puziy AM, Poddubnaya OI, Sevastyanova O, Serrano L, Luque R, Sels B (2018) Carbon Materials from Technical Lignins: Recent Advances. Top Curr Chem 376:1–34. https://doi.org/10.1007/S41061-018-0210-7
25. Zhang W, Yin J, Wang C, Zhao L, Jian W, Lu K, Lin H, Qiu X, Alshareef HN (2021) Lignin Derived Porous Carbons: Synthesis Methods and Supercapacitor Applications. Small Methods. https://doi.org/10.1002/SMTD.202100896
26. Jeon JW, Zhang L, Lutkenhaus JL, Laskar DD, Lemmon JP, Choi D, Nandasiri MI, Hashmi A, Xu J, Motkuri RK, Fernandez CA, Liu J, Tucker MP, McGrail PB, Yang B, Nune SK (2015) Controlling porosity in lignin-derived nanoporous carbon for supercapacitor applications. Chemsuschem 8:428–432. https://doi.org/10.1002/cssc.201402621
27. Madhu R, Periasamy AP, Schlee P, Hérou S, Titirici M-M (2023) Lignin: A sustainable precursor for nanostructured carbon materials for supercapacitors. Carbon N Y. https://doi.org/10.1016/J.CARBON.2023.03.001
28. Carrott P, Ribeiro Carrott M (2006) Lignin-From natural adsorbent to activated carbon: A review. Bioresour Technol 98:2301–2312. https://doi.org/10.1016/j.biortech.2006.08.008
29. Martin-Martinez M, Barreiro MFF, Silva AMT, Figueiredo JL, Faria JL, Gomes HT (2017) Lignin-based activated carbons as metal-free catalysts for the oxidative degradation of 4-nitrophenol in aqueous solution. Appl Catal B 219:372–378. https://doi.org/10.1016/j.apcatb.2017.07.065
30. Widsten P, Salo S, Hakkarainen T, Nguyen TL, Borrega M, Fearon O (2023) Antimicrobial and Flame-Retardant Coatings Prepared from Nano- and Microparticles of Unmodified and Nitrogen-Modified Polyphenols. Polymers (Basel) 15:992. https://doi.org/10.3390/POLYM15040992/S1
31. Castro-Gutiérrez J, Celzard A, Fierro V (2020) Energy Storage in Supercapacitors: Focus on Tannin-Derived Carbon Electrodes. Front Mater. https://doi.org/10.3389/FMATS.2020.00217
32. Castro-Gutiérrez J, Díez N, Sevilla M, Izquierdo MT, Ghanbaja J, Celzard A, Fierro V (2019) High-Rate Capability of Supercapacitors Based on Tannin-Derived Ordered Mesoporous Carbons. ACS Sustain Chem Eng 7:17627–17635. https://doi.org/10.1021/ACSSUSCHEMENG.9B03407
33. Pérez-Rodríguez S, Pinto O, Izquierdo MT, Segura C, Poon PS, Celzard A, Matos J, Fierro V (2021) Upgrading of pine tannin biochars as electrochemical capacitor electrodes. J Colloid Interface Sci 601:863–876. https://doi.org/10.1016/J.JCIS.2021.05.162
34. Sanchez-Sanchez A, Izquierdo MT, Medjahdi G, Ghanbaja J, Celzard A, Fierro V (2018) Ordered mesoporous carbons obtained by soft-templating of tannin in mild conditions. Microporous Mesoporous Mater 270:127–139. https://doi.org/10.1016/J.MICROMESO.2018.05.017
35. Castro-Gutiérrez J, Díez N, Sevilla M, Izquierdo MT, Celzard A, Fierro V (2021) Model carbon materials derived from tannin to assess the importance of pore connectivity in supercapacitors. Renew Sustain Energy Rev. https://doi.org/10.1016/J.RSER.2021.111600
36. Castro-Gutiérrez J, Sanchez-Sanchez A, Ghanbaja J, Díez N, Sevilla M, Celzard A, Fierro V (2018) Synthesis of perfectly ordered mesoporous carbons by water-assisted mechanochemical self-assembly of tannin. Green Chem 20:5123–5132. https://doi.org/10.1039/C8GC02295J
37. Inagaki M, Toyoda M, Soneda Y, Morishita T (2018) Nitrogen-doped carbon materials. Carbon N Y 132:104–140. https://doi.org/10.1016/j.carbon.2018.02.024
38. Sevilla M, Mokaya R (2014) Energy storage applications of activated carbons: Supercapacitors and hydrogen storage. Energy Environ Sci 7:1250–1280. https://doi.org/10.1039/C3EE43525C
39. Guo J, Morris JR, Ihm Y, Contescu CI, Gallego NC, Duscher G, Pennycook SJ, Chisholm MF (2012) Topological defects: origin of nanopores and enhanced adsorption performance in nanoporous carbon. Small 8:3283–3288. https://doi.org/10.1002/smll.201200894
40. R. Dupuis, P.L. Valdenaire, R.J.M. Pellenq, K. Ioannidou (2022) How chemical defects influence the charging of nanoporous carbon supercapacitors, Proc Natl Acad Sci U S A. 119: e2121945119. doi:https://doi.org/10.1073/PNAS.2121945119/SUPPL_FILE/PNAS.2121945119.SM01.MOV.
41. Liu Y, Wilcox J (2012) Molecular simulation of CO_2 adsorption in micro- and mesoporous carbons with surface heterogeneity. Int J Coal Geol 104:83–95. https://doi.org/10.1016/j.coal.2012.04.007
42. Babu DJ, Bruns M, Schneider R, Gerthsen D, Schneider JJ (2017) Understanding the influence of N-doping on the CO2 adsorption characteristics in carbon nanomaterials. J Phys Chem C 121:616–626. https://doi.org/10.1021/acs.jpcc.6b11686
43. Bandosz TJ, Seredych M, Rodríguez-Castellón E, Cheng Y, Daemen LL, Ramírez-Cuesta AJ (2016) Evidence for CO2 reactive adsorption on nanoporous S- and N-doped carbon at ambient conditions. Carbon N Y 96:856–863. https://doi.org/10.1016/j.carbon.2015.10.007
44. Seredych M, Jagiello J, Bandosz TJ (2014) Complexity of CO2 adsorption on nanoporous sulfur-doped carbons - Is surface chemistry an important factor? Carbon N Y 74:207–217. https://doi.org/10.1016/j.carbon.2014.03.024
45. Deng S, Wei H, Chen T, Wang B, Huang J, Yu G (2014) Superior CO2 adsorption on pine nut shell-derived activated carbons and the effective micropores at different temperatures. Chem Eng J 253:46–54. https://doi.org/10.1016/j.cej.2014.04.115
46. Ghimbeu CM, Górka J, Simone V, Simonin L, Martinet S, Vix-Guterl C (2017) Insights on the Na + ion storage mechanism in hard carbon: discrimination between the porosity, surface functional groups and defects. Nano Energy. https://doi.org/10.1016/j.nanoen.2017.12.013
47. Shao H, Wu YC, Lin Z, Taberna PL, Simon P (2020) Nanoporous carbon for electrochemical capacitive energy storage. Chem Soc Rev 49:3005–3039. https://doi.org/10.1039/D0CS00059K
48. J. Chmiola, G. Yushin, Y. Gogotsi, C. Portet, P. Simon, P.L. Taberna (2006) Anomalous increase in carbon at pore sizes less than 1 nanometer, Science (1979). 313:1760–1763. doi:https://doi.org/10.1126/SCIENCE.1132195.

49. Hayashi J, Kazehaya A, Muroyama K, Watkinson AP (2000) Preparation of activated carbon from lignin by chemical activation. Carbon N Y 38:1873–1878. https://doi.org/10.1016/S0008-6223(00)00027-0
50. Sun Y, Wei J, Wang YS, Yang G, Zhang JP (2010) Production of activated carbon by K2CO3 activation treatment of cornstalk lignin and its performance in removing phenol and subsequent bioregeneration. Environ Technol 31:53–61. https://doi.org/10.1080/09593330903338411
51. Xi Y, Yang D, Qiu X, Wang H, Huang J, Li Q (2018) Renewable lignin-based carbon with a remarkable electrochemical performance from potassium compound activation. Ind Crops Prod 124:747–754. https://doi.org/10.1016/J.INDCROP.2018.08.018
52. Tsubouchi N, Nishio M, Mochizuki Y (2016) Role of nitrogen in pore development in activated carbon prepared by potassium carbonate activation of lignin. Appl Surf Sci 371:301–306. https://doi.org/10.1016/J.APSUSC.2016.02.200
53. Díez N, Ferrero GA, Sevilla M, Fuertes AB (2019) A sustainable approach to hierarchically porous carbons from tannic acid and their utilization in supercapacitive energy storage systems. J Mater Chem A Mater 7:14280–14290. https://doi.org/10.1039/C9TA01712G
54. Sevilla M, Díez N, Fuertes AB (2021) More Sustainable Chemical Activation Strategies for the Production of Porous Carbons. Chemsuschem 14:94–117. https://doi.org/10.1002/CSSC.202001838
55. D.A. Khuong, T.T. Kieu, Y. Nakaoka, T. Tsubota, D. Tashima, H.N. Nguyen, D. Tanaka (2022) The investigation of activated carbon by K2CO3 activation: Micropores- and macropores-dominated structure, Chemosphere. 299: 134365. doi:https://doi.org/10.1016/J.CHEMOSPHERE.2022.134365.
56. Hayashi J, Horikawa T, Takeda I, Muroyama K, Nasir Ani F (2002) Preparing activated carbon from various nutshells by chemical activation with K2CO3. Carbon N Y 40:2381–2386. https://doi.org/10.1016/S0008-6223(02)00118-5
57. Hayashi J, Uchibayashi M, Horikawa T, Muroyama K, Gomes VG (2002) Synthesizing activated carbons from resins by chemical activation with K2CO3. Carbon N Y 40:2747–2752. https://doi.org/10.1016/S0008-6223(02)00151-3
58. Mahamud MM, Menéndez JM, Sarquís PE (2014) CO_2 activation of chars: Effect of burn-off on texture and fractal properties. Fuel Process Technol 119:41–51. https://doi.org/10.1016/j.fuproc.2013.10.009
59. Allen SJ, Whitten L, McKay G (1998) The Production and Characterisation of Activated Carbons: A Review. Dev Chem Eng Miner Process 6:231–261. https://doi.org/10.1002/APJ.5500060501
60. H. Marsh, F. Rodriguez-Reinoso (2006) Activated Carbon, Elsevier Science & Technology Books.
61. Sajjadi B, Chen WY, Egiebor NO (2019) A comprehensive review on physical activation of biochar for energy and environmental applications. Rev Chem Eng 35:735–776. https://doi.org/10.1515/revce-2017-0113
62. D. Bergna, T. Varila, H. Romar, U. Lassi (2022) Activated carbon from hydrolysis lignin: Effect of activation method on carbon properties, Biomass Bioenergy. 159: 106387. doi:https://doi.org/10.1016/J.BIOMBIOE.2022.106387.
63. Wang Z, Wang F, Cao J, Wang J (2010) Pyrolysis of pine wood in a slowly heating fixed-bed reactor: Potassium carbonate versus calcium hydroxide as a catalyst. Fuel Process Technol 91:942–950. https://doi.org/10.1016/J.FUPROC.2009.09.015
64. Rutkowski P (2011) Pyrolysis of cellulose, xylan and lignin with the K2CO3 and ZnCl2 addition for bio-oil production. Fuel Process Technol 92:517–522. https://doi.org/10.1016/J.FUPROC.2010.11.006
65. Jalalabadi T, Drewery M, Tremain P, Wilkinson J, Moghtaderi B, Allen J (2020) The impact of carbonate salts on char formation and gas evolution during the slow pyrolysis of biomass, cellulose, and lignin. Sustain Energy Fuels 4:5987–6003. https://doi.org/10.1039/D0SE01031F
66. Gierer J (1980) Chemical aspects of kraft pulping. Wood Sci Technol 14:241–266. https://doi.org/10.1007/BF00383453
67. Sixta H, Potthast A, Krotschek AW (2006) Chemical Pulping Processes. Handbook of Pulp. https://doi.org/10.1002/9783527619887.ch4a
68. Li J, Gellerstedt G, Toven K (2009) Steam explosion lignins; their extraction, structure and potential as feedstock for biodiesel and chemicals. Bioresour Technol 100:2556–2561. https://doi.org/10.1016/J.BIORTECH.2008.12.004
69. Suota MJ, da Silva TA, Zawadzki SF, Sassaki GL, Hansel FA, Paleologou M, Ramos LP (2021) Chemical and structural characterization of hardwood and softwood LignoForce™ lignins. Ind Crops Prod. https://doi.org/10.1016/j.indcrop.2021.114138
70. H. Wikberg, T. Ohra-Aho, Leppävuori.Juha, T. Liitiä, H. Kanerva (2018) Method for producing reactive lignin WO2018115592A1.
71. Pöhler T, Widsten P, Hakkarainen T (2022) Improved Fire Retardancy of Cellulose Fibres via Deposition of Nitrogen-Modified Biopolyphenols. Molecules 27:3741. https://doi.org/10.3390/MOLECULES27123741
72. Varila T, Brännström H, Kilpeläinen P, Hellström J, Romar H, Nurmi J, Lassi U (2020) From Norway Spruce Bark to Carbon Foams : Characterization, and Applications. BioResources 15:3651–3666. https://doi.org/10.15376/BIORES.15.2.3651-3666
73. Matsukata M, Fujikawa T, Kikuchi E, Morita Y (1988) Interaction Between Potassium Carbonate and Carbon Substrate at Subgasification Temperatures. Migration of Potassium into the Carbon Matrix, Energy and Fuels 2:750–756. https://doi.org/10.1021/EF00012A006/ASSET/EF00012A006.FP.PNG_V03
74. Domínguez-Robles J, Tamminen T, Liitiä T, Peresin MS, Rodríguez A, Jääskeläinen AS (2018) Aqueous acetone fractionation of kraft, organosolv and soda lignins. Int J Biol Macromol 106:979–987. https://doi.org/10.1016/J.IJBIOMAC.2017.08.102
75. Jääskeläinen AS, Liitiä T, Mikkelson A, Tamminen T (2017) Aqueous organic solvent fractionation as means to improve lignin homogeneity and purity. Ind Crops Prod 103:51–58. https://doi.org/10.1016/j.indcrop.2017.03.039
76. Lu C, Xu S, Liu C (2010) The role of K2CO3 during the chemical activation of petroleum coke with KOH. J Anal Appl Pyrolysis 87:282–287. https://doi.org/10.1016/J.JAAP.2010.02.001
77. Strange JF, Walker PL (1976) Carbon-carbon dioxide reaction: Langmuir-Hinshelwood kinetics at intermediate pressures. Carbon N Y 14:345–350. https://doi.org/10.1016/0008-6223(76)90008-7
78. Crestini C, Lange H, Sette M, Argyropoulos DS (2017) On the structure of softwood kraft lignin. Green Chem 19:4104–4121. https://doi.org/10.1039/C7GC01812F
79. Pienihäkkinen E, Lindfors C, Ohra-Aho T, Lehtonen J, Granström T, Yamamoto M, Oasmaa A (2021) Fast Pyrolysis of Hydrolysis Lignin in Fluidized Bed Reactors. Energy Fuels 35:14758–14769. https://doi.org/10.1021/ACS.ENERGYFUELS.1C01719/ASSET/IMAGES/LARGE/EF1C01719_0012.JPEG
80. Mermoud F, Golfier F, Salvador S, Vandesteene L, Dirion J (2006) Experimental and numerical study of steam gasification of a single charcoal particle. Combust Flame 145:59–79. https://doi.org/10.1016/j.combustflame.2005.12.004
81. Sircar I, Sane A, Wang W, J.P. (2014) Gore, Experimental and modeling study of pinewood char gasification with CO2. Fuel 119:38–46. https://doi.org/10.1016/j.fuel.2013.11.026
82. Yamashita T, Fujii Y, Morozumi Y, Aoki H, Miura T (2006) Modeling of gasification and fragmentation behavior of char particles

having complicated structures. Combust Flame 146:85–94. https://doi.org/10.1016/j.combustflame.2006.04.009
83. Raymundo-Piñero E, Azaïs P, Cacciaguerra T, Cazorla-Amorós D, Linares-Solano A, Béguin F (2005) KOH and NaOH activation mechanisms of multiwalled carbon nanotubes with different structural organisation. Carbon N Y 43:786–795. https://doi.org/10.1016/j.carbon.2004.11.005
84. W. Chen, M. Gong, K. Li, M. Xia, Z. Chen, H. Xiao, Y. Fang, Y. Chen, H. Yang, H. Chen (2020) Insight into KOH activation mechanism during biomass pyrolysis: Chemical reactions between O-containing groups and KOH, Appl Energy. 278 :115730. doi:https://doi.org/10.1016/J.APENERGY.2020.115730.
85. Karlström O, Brink A, Hupa M (2015) Desorption kinetics of CO in char oxidation and gasification in O2, CO2 and H2O. Combust Flame 162:788–796. https://doi.org/10.1016/j.combustflame.2014.08.010
86. A.K. Burnham (2017) Global Chemical Kinetics of Fossil Fuels: How to Model Maturation and Pyrolysis, Global Chemical Kinetics of Fossil Fuels: How to Model Maturation and Pyrolysis. doi:https://doi.org/10.1007/978-3-319-49634-4/COVER.
87. Nordeng SH (2019) The statistical compensation effect in nonisothermal kinetics: Theory, simulations and experimental evidence. Org Geochem 127:124–135. https://doi.org/10.1016/J.ORGGEOCHEM.2018.11.005
88. P.J. Barrie, The mathematical origins of the kinetic compensation effect: 1. the effect of random experimental errors, Physical Chemistry Chemical Physics. 14:318–326 (2011). doi:https://doi.org/10.1039/C1CP22666E.
89. P.J. Barrie, The mathematical origins of the kinetic compensation effect: 2. the effect of systematic errors, Physical Chemistry Chemical Physics. 14 : 327–336 (2011). doi:https://doi.org/10.1039/C1CP22667C.
90. Agrawal RK (1986) On the compensation effect. J Therm Anal 31:73–86. https://doi.org/10.1007/BF01913888/METRICS
91. Harvey JP, Saadatkhah N, Dumont-Vandewinkel G, Ackermann SLG, Patience GS (2018) Experimental methods in chemical engineering: Differential scanning calorimetry—DSC. Can J Chem Eng 96:2518–2525. https://doi.org/10.1002/CJCE.23346
92. C. Guizani, F.J. Escudero Sanz, S. Salvador, Influence of temperature and particle size on the single and mixed atmosphere gasification of biomass char with H2O and CO2, Fuel Processing Technology. 134 : 175–188 (2015). doi:https://doi.org/10.1016/j.fuproc.2015.01.031.
93. C. Dupont, T. Nocquet, J.A. Da Costa, C. Verne-Tournon (2011) Kinetic modelling of steam gasification of various woody biomass chars: influence of inorganic elements. Bioresour Technol. 102: 9743–9748. doi:https://doi.org/10.1016/j.biortech.2011.07.016.
94. Umemoto S, Kajitani S, Hara S (2013) Modeling of coal char gasification in coexistence of CO_2 and H_2O considering sharing of active sites. Fuel 103:14–21. https://doi.org/10.1016/j.fuel.2011.11.030
95. Numazawa Y, Hara Y, Matsukawa Y, Matsushita Y, Aoki H, Shishido T, Okuyama N (2021) Kinetic modeling of CO_2 and H_2O gasification reactions for metallurgical coke using a distributed activation energy model. ACS Omega 6:11436–11446. https://doi.org/10.1021/ACSOMEGA.1C00443/ASSET/IMAGES/LARGE/AO1C00443_0011.JPEG
96. Fritz OW, Hüttinger KJ (1993) Active sites and intrinsic rates of carbon-gas reactions—a definite confirmation with the carbon-carbon dioxide reaction. Carbon N Y 31:923–930. https://doi.org/10.1016/0008-6223(93)90193-E